International Journal of Heat and Mass Transfer 112 (2017) 699–708

Contents lists available at ScienceDirect

International Journal of Heat and Mass Transfer

journal homepage: www.elsevier.com/locate/ijhmt

An experimental investigation on heat transfer enhancement of sprayed wire-mesh heat exchangers

Yanchen Fu, Jie Wen *, Cuizhen Zhang

National Key Laboratory of Science and Technology on Aero-Engine Aero-thermodynamics, Collaborative Innovation Center of Advanced Aero-Engine, School of Energy and Power Engineering, Beihang University, Beijing 100191, China

ARTICLE INFO

Article history:
Received 28 December 2016
Received in revised form 6 April 2017
Accepted 7 May 2017

Keywords:
Heat transfer enhancement
Wire-arc spray
Wire mesh
Heat exchanger

ABSTRACT

Three different porosities of aluminum wire meshes (10PPI, 14PPI, 20PPI) and three different diameters of aluminum wires were used to fabricate heat exchangers by connecting aluminum tubes to increase the heat transfer surface area. A twin wire-arc thermal spraying system can generate a dense, high strength aluminum coating to connect wires and aluminum tube. Tiled and clamped connections between the wire mesh and tube were applied to obtain an efficient heat exchanger. The heat transfer characteristics for plain tube, three sprayed tube-wire and six sprayed wire-meshes (SPW) heat exchangers were experimentally tested. Also, heat exchanger surface temperatures were measured using infrared camera. Ideal fin model was applied after validation using data of sprayed tube-wire heat exchangers. The tube inlet temperature ranged from 100 to 200 °C and the wind tunnel air velocity was from 2 to 20 m/s. The results indicate that all the SPW heat exchangers can enhance the heat transfer compared with plain tube heat exchanger. Tube outside Nusselt number was fitted with Reynolds number and wire mesh porosity. 20PPI clamped SPW was suggested to be used in the future design of compact heat exchangers due to the maximum 76.7% equivalent efficiency compared with ideal fin model.

1. Introduction

Compact heat exchangers are widely used in various applications, including air-conditioning evaporators and condensers, electronic cooling devices, waste heat recovery system and cryogenic exchangers [1]. To meet the needs of lightweight, space-saving and economical, extended surfaces with large surface area/volume ratios are normally applied in compact heat exchangers [2–4]. The large surface area is seized on the fin side since there exists lower heat transfer coefficient. Also, the fins attached with the wall can separate the two fluids and enhance the flow turbulences.

Metal foams, perforated sheets and wire meshes are equipped and researched in the compact heat exchangers these decades [5–8]. Open cell metal foam has high specific surfaces, relative high thermal conductivity and can also promote mixing when fluids flow through it. Mancin et al. [9] carried out heat transfer and pressure drop measurements during air forced convection through five different copper samples. The results demonstrate that heat transfer coefficient does not depend on the imposed heat flux and it increases with the increase of air mass flow rate. Besides, the pressure drop is higher with larger pore density. White et al. [10] presented a novel numerical modeling technique for perforated plate heat exchangers that the model allows each perforated plate to be modeled in detail. However, this method retains computational efficiency by using nodes exponentially concentrated near the edge of perforated plates. The numerical results are well matched with the experimental data applied in the silicon heat exchanger plates and glass spacers. Furthermore, pressure drops of four plain-square type woven metal screens with various porosities were experimented in Wu study [11]. It is estimated that the velocity developing section is relatively short for woven metal screens. The five new frictional factor empirical equations for various types of metal screens were presented in the study. Many other researchers have extensively studied on the fluid flow and heat transfer characteristics of porous media structures by experimental [12–21], numerical [22–27] and analytical methods [28,29]. Plenty of results can be used in the design and measurements of compact heat exchangers.

On the basis of previous research, one method to fabricate heat exchanger with porous media using thermal spray process has been effectively applied. Jazi et al. [30] sprayed to deposit Inconel 625 skins on the surface 10 and 20 pores per inch (PPI) nickel foams. A ceramic thermal barrier coating was deposited by plasma spraying to fabricate the heat exchanger. Flow and heat transfer characteristics were obtained when the air flows through heat exchangers. Tsolas and Chandra [31] used wire-arc thermal spray

* Corresponding author.
E-mail address: wenjie@buaa.edu.cn (J. Wen).

http://dx.doi.org/10.1016/j.ijheatmasstransfer.2017.05.026
0017-9310/

Nomenclature

A	tube section area (m^2)
Cp	isobaric specific heat capacity (kJ/kg °C)
D	wire diameter (m)
d	tube diameter (m)
h	heat transfer coefficient (W/m^2 °C)
l	wire length (m)
m	mass flow rate (kg/s)
Nu	Nusselt number
P	wire perimeter (m)
Pr	Prandtl number
q	heat transfer rate (W)
Re	Reynolds number
T	temperature (°C)
U	overall heat transfer coefficient (W/m^2 °C)
u	flow velocity (m/s)
x	distance (m)

Greek

μ	dynamic viscosity (Pa s)
ρ	density (kg/m^3)
ε	wire mesh porosity
λ	thermal conductivity (W/m °C)
η	correction factor
ξ	SPW heat exchanger efficiency

Subscripts

c	cross section
$LMTD$	logarithmic mean temperature difference
m	wire mesh
in	inlet
i	inner
out	outlet
o	outer
p	plain tube
w	wind tunnel side
s	base surface
t	tube side

Abbreviation

PPI	pore per inch
SPW	sprayed wire mesh

to deposit 2 mm thick metal skins on the surface of 10PPI and 40PPI nickel and copper foams. Pressure drop and temperature distribution were measured as the compressed air was blown through the foams. The results show that the heat transfer enhances nearly 7 times compared with the hollow tube and new friction factor correlation is updated with the permeability K and inertial coefficient C_F. Moreover, the wire mesh was tightly connected with the heat exchanger tube as the surface of the wire mesh and tubes were deposited coating using wire-arc thermal spraying in Rezaey et al. [32] research. This kind of heat exchanger is helpful to recover heat from hot combustion gases using cooling water and the maximum of 68% higher temperature rise is seized compared with plain tubes.

To recycle the waste heat of gas oven, aluminum U-tube heat exchangers were fabricated using wires and wire meshes. Wire mesh was tiled and clamped connected by coating sprayed using wire-arc thermal spraying system. Coating characteristics were analyzed in terms of scanning electron microscope and energy dispersive X-ray spectroscopy (SEM-EDS) technology and spraying parameters were controlled to obtain better bonding effect. Heat transfer characteristics were measured and calculated under various wind tunnel velocities. Pictures of heat exchanger tube surface temperature and heat transfer rate were analyzed to compare with fin model. Moreover, tube-outside heat transfer enhancement was significantly observed for different porosities of wire meshes.

2. Experimental description

2.1. Experimental apparatus

Fig. 1 presents the schematic diagram of experimental setup where the cooling air flowed over various heat exchangers.

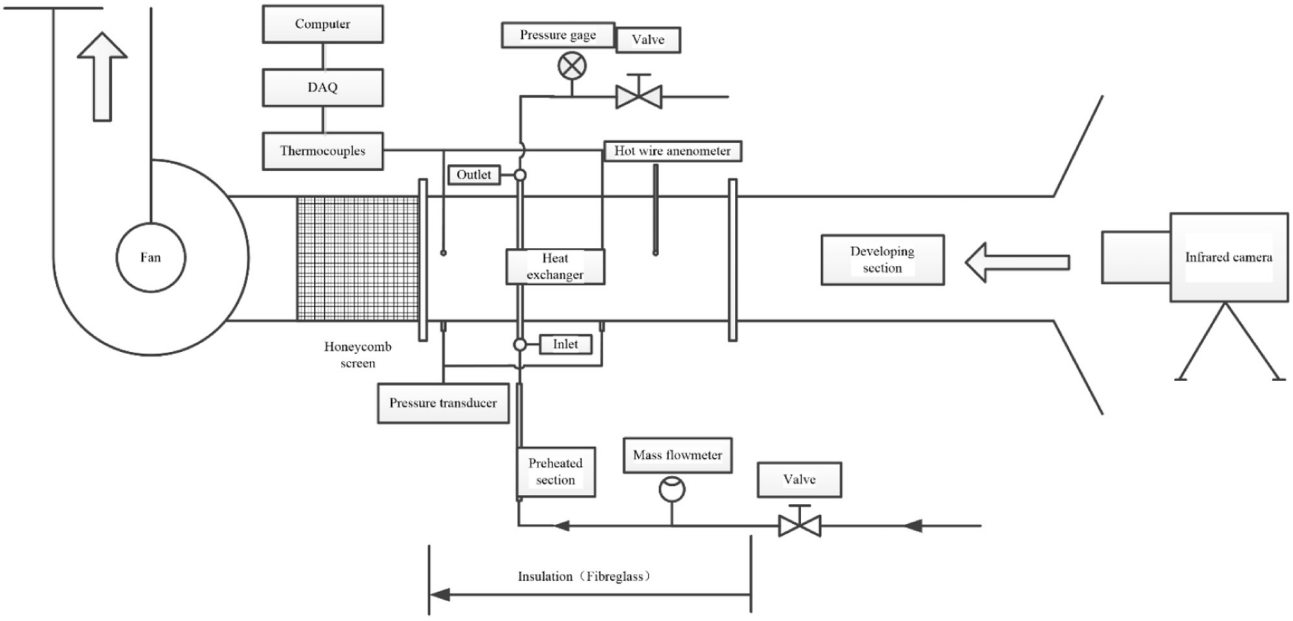

Fig. 1. Schematic diagram of heat exchanger experimental setup.

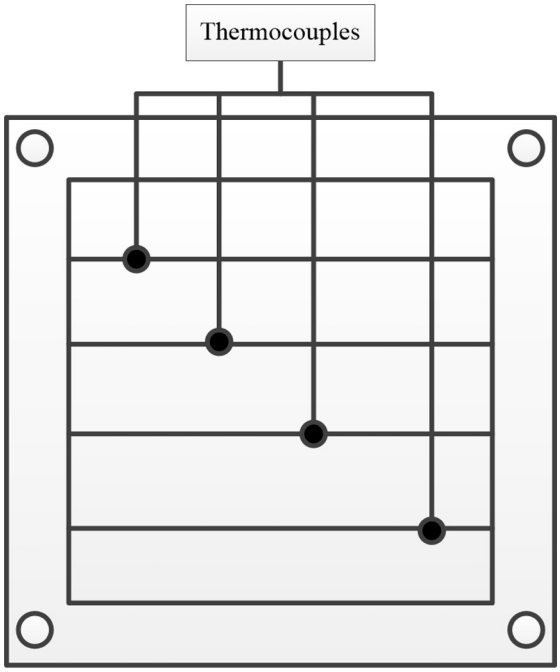

Fig. 2. Wind tunnel air thermocouples distribution.

The airflow was generated by an exhauster (single phase motor, Plint & Partner. Ltd. UK) with the maximum velocity up to 20 m/s. The wind tunnel has a rectangular air duct with a cross-sectional area of 127 mm × 127 mm and the heat exchanger is located in the center of the duct. Cooling air velocity was measured using an anemometer (hot wire type, Omega) located in front of the tube bundle. The range of the flow velocity varied in 2–20 m/s with the measurement error of 0.1 m/s. In order to create a developed air flow across the test section, 0.9 m long channel with honeycomb installed was used to mix air in the upstream. Four K-type thermocouples with ±0.5 °C accuracy were arranged to measure the air stream temperature as shown in Fig. 2. 8 K-type thermocouples were set uniformly on the top and bottom shells of the duct measuring shell wall temperatures to estimate the heat loss at the shell side. The infrared camera (SC 5000, Flir Company) was set at the inlet of the wind tunnel to measure the heat exchanger base surface temperature and the images of temperature distribution was acquired to the laptop through the data cable. All heat exchangers were painted in black and emissivity was calibrated before the test. The whole test section was wrapped with fiberglass insulation to minimize the heat loss to the surroundings.

For the hot air side, the air volumetric flow rate was measured by a gas mass controller (FMA5400, 0–100 L/min, and Omega) and the flow rate was fixed to 20 L/min during the whole experiments. The preheated section consisting of a tube and a heat tape (120VAC, maximum 208 W) was connected to compressed air supply in order to heat air to the range of 100–200 °C. Two armed K-type thermocouples with ±0.5 °C accuracy can measure the tube side inlet and outlet temperatures. A constant air bath was provided by a compressor (Sigma Air tower, Kaeser) and the path pressure was fixed at the pressure of 0.45 MPa by the regulation of two valves in the path. All the data of thermocouples was recorded to the computer through a National Instruments Data Acquisition

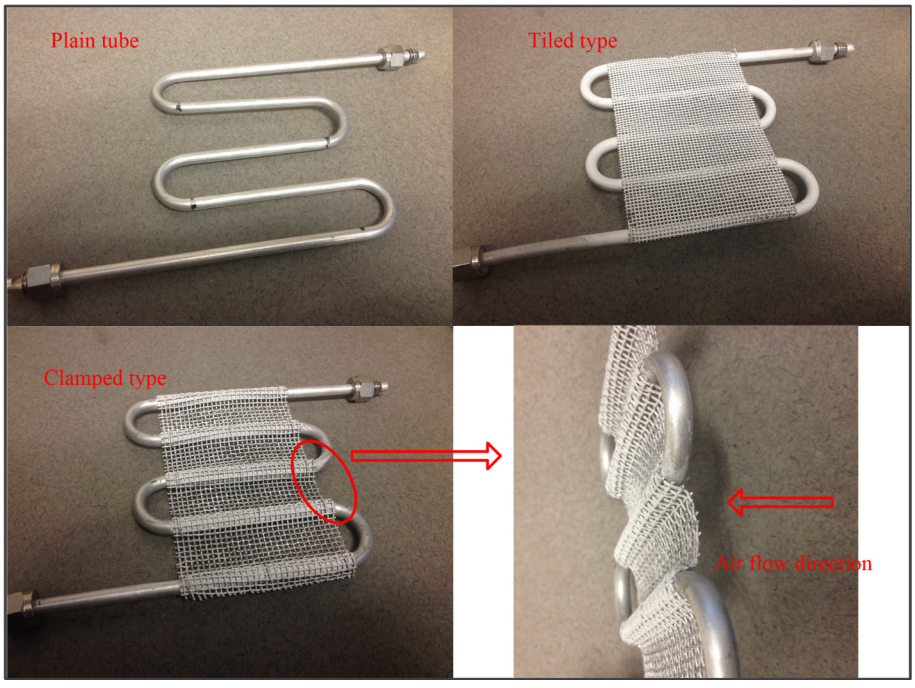

Fig. 3. Sample pictures of three types of heat exchangers.

Table 1
Experimental test conditions.

Wind tunnel side		Tube side	
Air velocity (m/s)	2, 5, 8, 10, 15, 20	Volumetric flow rate (L/min)	20.00
Pressure (MPa)	0.10	Pressure (MPa)	0.45
Temperature (°C)	Room temperature	Inlet temperature (°C)	100, 130, 150, 180, 200

Table 2
Geometrical features of tested heat exchangers.

Bare tube			Wire	Wire mesh
Inner diameter (mm)	4.72	Diameter (mm)	0.81, 1.62, 2.05	/
Outer diamter (mm)	6.35	Size (PPI)	/	10, 14, 20
Straight length (m)	0.11	Width (mm)	76.2	
Bending diamter (mm)	24.4	Height (mm)	127	

(DAQ) unit and software of Lab-view Signal Express V3.0. The tube side volumetric flow rate and wind tunnel velocity can be seized on the instrument screen displays. The detailed test conditions were shown in Table 1.

2.2. Fabrication of heat exchangers

Fig. 3 shows pictures of plain tube, tiled and clamped type of SPW heat exchangers. In the test section, all SPW heat exchangers were set that the tube surface is vertical to the windward side and the air flow direction can be indicated in the last panel. The heat exchangers use aluminum (Al) tubes with an inner and outer diameter of 4.72 mm and 6.35 mm. Al wire meshes were shaped to rectangle of 76.2 mm × 127 mm, which could exactly cover the straight section of the plain tube. Three sizes of Al plain weaves wire mesh were used to connect the plain tubes: 10PPI, 14PPI and 20PPI, corresponding to the porosity of 79.8%, 77.0% and 73.6%, respectively. The method to calculate the porosity can be seen in the previous search [16]. The wire mesh was wrapped around the tube and then sand blasted to be sprayed for the better connection. Furthermore, three different diameters of aluminum wires (0.81 mm, 1.62 mm, 2.05 mm) were used to form another types of heat exchanger. Single wires were tied up onto the surface of the parallel straight tube section uniformly. The connected sections were sand blasted and then sprayed using aluminum coating

Table 3
Wire-arc thermal spray parameters for deposition of aluminum coating.

Parameter	Value
Torch	Wire arc
Wire feed rate (m/min)	6.5
Voltage (V)	32.9
Inlet pressure (MPa)	0.55
Air flow rate (L/min)	1.7
Spraying distance (m)	0.15

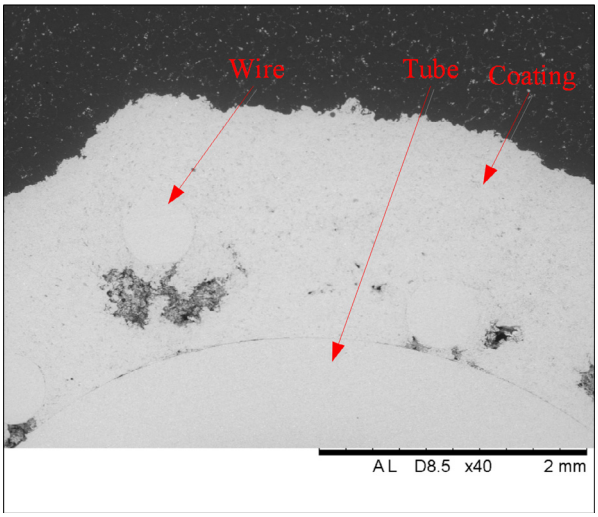

Fig. 4. Aluminum coating connection quality.

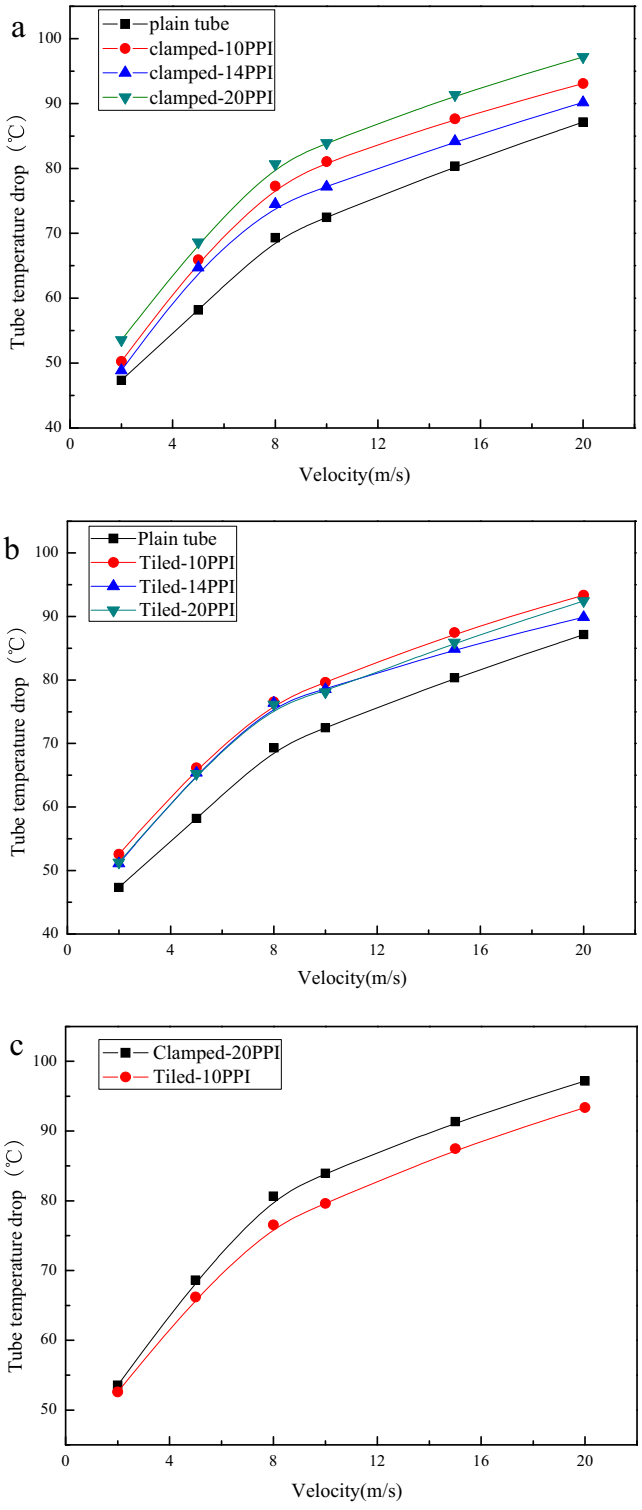

Fig. 5. Tube temperature drop through SPW heat exchangers compared with the plain tube under various velocities.

to make better bonding as mentioned above. Five Al wires with identical diameter were distributed uniformly in the tube straight section. Thus, sprayed tube-wire heat exchangers including three different aluminum wire diameters were fabricated and their details are shown in Table 2.

Al wire mesh and wires were sprayed using a twin wire-arc spraying system (Valu-Arc, Sulzer Metco Inc., Westbury, NY) to produce better connection between the wire and the tube. The chosen wire-arc thermal spray parameters for deposition of aluminum is shown in Table 3. Furthermore, some samples sprayed on the heat exchanger was made to examine the coating and bonding characteristics using SEM-EDS (TM3000, Hitachi High-Technologies Canada Incorporated, Toronto, ON). The results are shown in Fig. 4 that there is no obvious interface between the wire and the tube.

3. Results and discussion

Flow and heat transfer characteristics were studied under 20 L/min tube side volume flow rate, 0.45 MPa pressure and at five various tube inlet temperatures ranging from 100 °C to 200 °C. The wind tunnel velocity ranges from 2 m/s to 20 m/s at seven different values to obtain the Reynolds number influences. Once the experimental test was activated, the temperature, pressure, and flow rate values were saved at least 10 min after all the test parameters were confirmed to reach the stable states. Fig. 5 shows the temperature drop of tube side for SPW heat exchangers and plain tube under various wind tunnel velocities. It is indicated that SPW heat exchangers have higher temperature drops and they have better cooling affect compared with the plain tube. Also, the temperature drop increases with the increase of wind tunnel velocity and the increasing slope tends to be flat when the velocity is larger than 8 m/s. For clamped type of SPW heat exchangers from Fig. 5(a), temperature drop is the lowest although the 14PPI has larger wire mesh surface area than 10PPI. The reason is concluded that this type has worse contact between the tube and wire mesh. Fig. 5 (b) shows the temperature drop for tiled SPW heat exchangers. As the connection is just one line between the tube and wire mesh, heat transfer is almost the same for different porosities of wire mesh. Fig. 5(c) obviously shows that 20PPI clamped SPW heat exchangers have the maximum temperature drop and the type of clamped can be used in the future SPW heat exchanger design.

Infrared camera is used to measure the surface temperatures of SPW heat exchanger and Fig. 6 displays temperature distributions for three types of clamped SPW heat exchangers under velocities of 2 m/s and 8 m/s. For all conditions of wind tunnel velocities, tube surface temperature distribution is almost linearly decreasing from the tube inlet to outlet. At the section of wrapped wire mesh, the surface temperature drops more sharply than that of bend section. It is explained that the wire mesh can be used to take much more heat from the tube surface and the SPW heat exchangers have better cooling effect than the plain tube.

3.1. Data reduction

Under the present experimental setup, the temperature data were collected to evaluate the wind tunnel side convective heat transfer characteristics for various types of heat exchangers. Heat transfer rate balance equations of heat exchanger are defined in the two following equations.

$$q_w = m_w Cp_w (T_{w,out} - T_{w,in}) \tag{1}$$

$$q_t = m_t Cp_t (T_{t,in} - T_{t,out}) \tag{2}$$

where the subscripts w and t represent wind tunnel and tube side. Subscripts *in* and *out* represent inlet and outlet, respectively. The heat loss for the whole experiment is mainly from the natural convection of wind tunnel shells. Based on the measured wind tunnel wall surface temperature and Nusselt number correlation at the infinite flat plate, value of heat loss is revised and the real heat rate transferred through the heat exchanger is confirmed. Then all the actual heat transfer rate can also be defined in terms of the overall heat transfer coefficient U and logarithmic mean temperature difference ΔT_{LMTD} as

$$q = UA_o \Delta T_{LMTD} \tag{3}$$

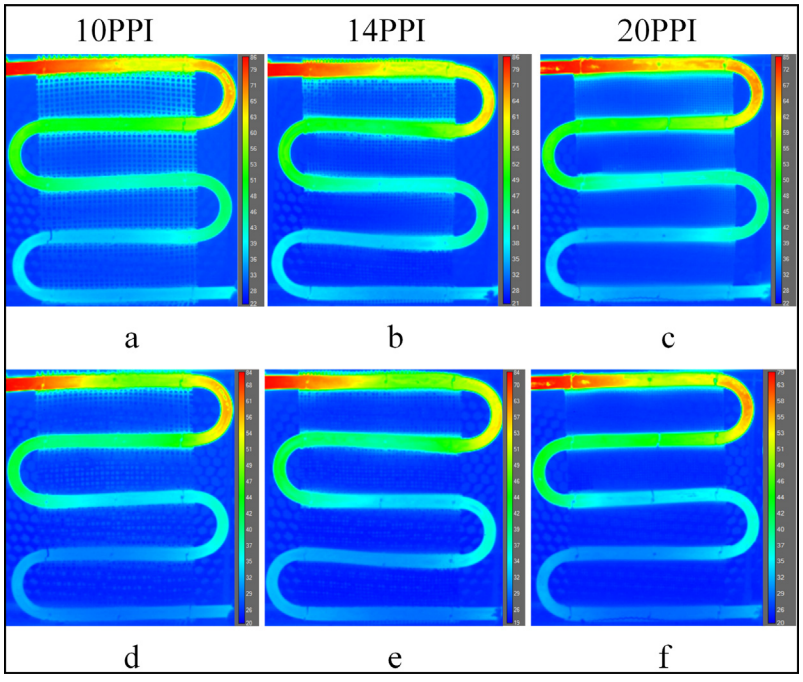

Fig. 6. Surface temperature distribution for clamped SPW heat exchangers. (Tube inlet temperature: 150 °C; wind tunnel velocity: a–c: 2 m/s; d–f: 8 m/s).

$$\Delta T_{LMTD} = \frac{\Delta T_2 - \Delta T_1}{\ln(\Delta T_2/\Delta T_1)} \tag{4}$$

where A_o represents the tube outer surface area including sprayed coating or not for different heat exchangers. ΔT_1 and ΔT_2 are defined as follows:

$$\Delta T_1 = T_{t,in} - T_{w,out} \tag{5}$$

$$\Delta T_2 = T_{t,out} - T_{w,in} \tag{6}$$

The overall heat transfer coefficient U can be defined related to the wind tunnel and tube side heat transfer coefficients h_w and h_t by the following equation:

$$\frac{1}{UA_o} = \frac{1}{h_w A_o} + \frac{1}{2\pi\lambda}\ln\frac{d_o}{d_i} + \frac{1}{h_t A_i} \tag{7}$$

where A_i and d_i are the internal surface area of heat exchanger tube and inner tube diameter, respectively. λ is the tube thermal conductivity that has the same value as the wind tunnel wall. As the hot air flows in the regular aluminum tube, the tube inside heat transfer coefficient can be calculated using classic Gnielinski formula [33] shown below,

$$h_t = \left(\frac{\lambda_t}{d_i}\right)\frac{(Re_t - 1000)Pr_t(f_t/2)}{1 + 12.7\sqrt{f_t/8}(Pr_t^{2/3} - 1)} \tag{8}$$

where f_t is the Darcy friction coefficient of the air and defined as the following equation:

$$f_t = (1.82\lg Re_t - 1.64)^{-2} \tag{9}$$

Re_t and Pr_t show Reynolds and Prandtl numbers at the tube side, respectively. The two values are calculated using following equations:

$$Re_t = \frac{\rho_t u_t d_i}{\mu_t} \tag{10}$$

$$Pr_t = \frac{Cp_t \mu_t}{\lambda_t} \tag{11}$$

where μ_t denotes the air velocity in the tube. Cp_t, ρ_t and μ_t represent the isobaric specific capacity, density and dynamic viscosity, respectively. Furthermore, the wind tunnel side convective heat transfer coefficient can be obtained using Eqs. (7) and (8). Nusselt number can be further calculated to analyze the wind tunnel side heat transfer of the normal plain tube and SPW heat exchangers using the following equation.

$$Nu_w = \frac{h_w d_o}{\lambda_w} \tag{12}$$

where d_o is the outer diameter of the heat exchanger tube, the equivalent diameter was revised for the SPW heat exchanger by adding wire diameter.

The direct measurements of this experiment and their uncertainties are shown in Table 4. As the total heat transfer amount is calculated by Eq. (2), its uncertainty is defined using the following equation according to error propagation under non-linear form.

$$\frac{\Delta q}{q} = \sqrt{\left(\frac{\Delta T_{t,in}}{T_{t,in}}\right)^2 + \left(\frac{\Delta T_{t,out}}{T_{t,out}}\right)^2 + \left(\frac{\Delta m_t}{m_t}\right)^2} = 7.5\% \tag{13}$$

Table 4
Uncertainty of the direct measurements.

Direct measurement	Measuring instrument	Measure uncertainty
Tube side volume flow rate	Gas mass controller	±1.5%
Wind tunnel velocity	Hot wire anemometer	0.1 m/s
Tube inlet and outlet temperature	K type sheathed thermocouple	0.5 °C
Wind tunnel temperature	K type thermocouple	0.5 °C
Tube diameter	Vernier caliper	0.02 mm

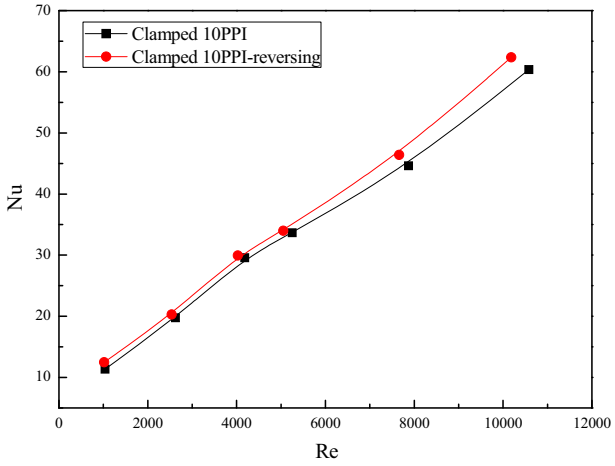

Fig. 7. *Nu* number variation with *Re* number of 10PPI clamped SPW heat exchangers under two set positions.

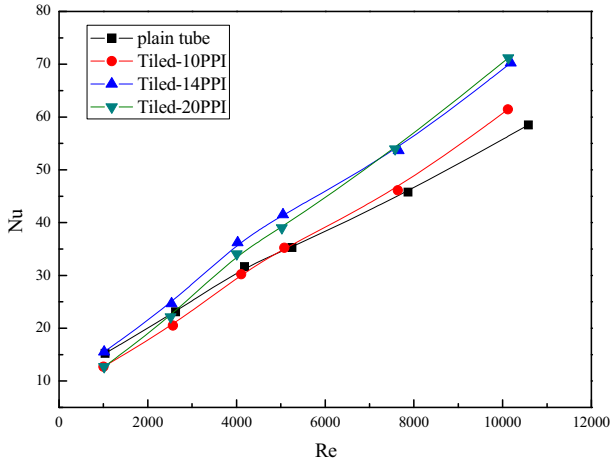

Fig. 8. *Nu* number variation with *Re* number for tiled SPW heat exchangers.

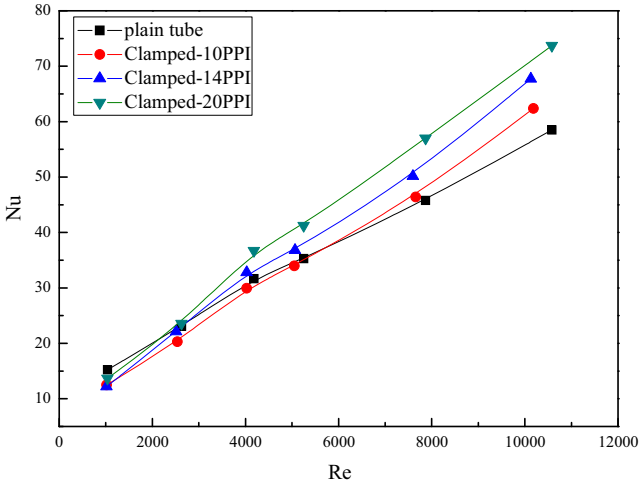

Fig. 9. *Nu* number variation with *Re* number for clamped SPW heat exchangers.

The maximum relative error of logarithmic mean temperature difference is calculated due to the Eq. (4) as 3.9%. Thus, the following equation shows the maximum relative error of overall heat transfer coefficient.

$$\frac{\Delta U}{U}=\sqrt{\left(\frac{\Delta T_{t,in}}{T_{t,in}}\right)^2+\left(\frac{\Delta T_{t,out}}{T_{t,out}}\right)^2+\left(\frac{\Delta m_t}{m_t}\right)^2+\left(\frac{\Delta(\Delta T_m)}{\Delta T_m}\right)^2}=8.4\% \tag{14}$$

According to Eqs. (8)–(11), the combined uncertainty of tube side heat transfer coefficient is calculated in the following equation.

$$\frac{\Delta h_t}{h_t}=\sqrt{\left(\frac{\Delta U}{U}\right)^2+\left(\frac{\Delta A_o}{A_o}\right)^2+\left(\frac{\Delta A_i}{A_i}\right)^2+\left(\frac{\Delta d_o}{d_o}\right)^2+\left(\frac{\Delta d_i}{d_i}\right)^2} \tag{15}$$

Considering all measurement uncertainties, the value of uncertainty is estimated to be 8.5% in all experimental conditions.

3.2. Tube outside heat transfer analysis

To evaluate the heat transfer enhancement for SPW heat exchangers, outside tube heat transfer of plain tube heat exchanger was measured under same conditions. The Zukauskas correlation [34] for the tube banks average heat transfer coefficient has been used to compare with experimental results.

$$Nu=\eta*0.25Re_w^{0.63}Pr_w^{0.36}\left(\frac{Pr_w}{Pr_s}\right)^{0.25} \tag{16}$$
$$\eta=0.7$$

The correction factor η is equal to 0.7 as the tube banks have only one layer. Pr_w and Pr_s represent the Prandtl numbers in terms of wind tunnel air and tube wall temperatures. The value of Pr_w/Pr_s can be considered as one due to the tiny difference between the two parameter values. The experimental results can generally match the empirical correlation with the average error of 3.9%. Thus, the accuracy of the experimental setup was verified for further various heat exchangers tests. Considering different windward sides of heat exchangers can influence the flow status and further make the heat transfer difference, 20PPI SPW heat exchangers was reversely set to test the heat transfer. Fig. 7 shows the Nusselt number variation with Reynolds number for clamped SPW heat exchangers under two different set positions. The clamped type can make large bonding area between the tube and wire mesh, which leads to the larger thermal contact resistance. Also, the air backflow accumulates at the backside of the heat exchangers when the air flows across the tube. On account of better convective heat transfer on the tube base surface under lower velocity conditions, the better heat exchanger setup that the leading edge is tube surface should be considered in the applications.

Fig. 8 shows the tube outside Nusselt number variation with *Re* number for tiled SPW heat exchangers. It is pointed that heat transfer always enhances because the plain tube equips with wire mesh and is sprayed aluminum coatings. The wire mesh connection enlarges the outside heat transfer area compared with plain tube. Extended wire can be considered as the fin to improve the tube surface conduction and then increase the convective heat transfer by wind tunnel flowing air. When the air flows across the cylinder tube, the turbulence extent improves due to the wire mesh disturbance in front of the tube. The figure also shows that

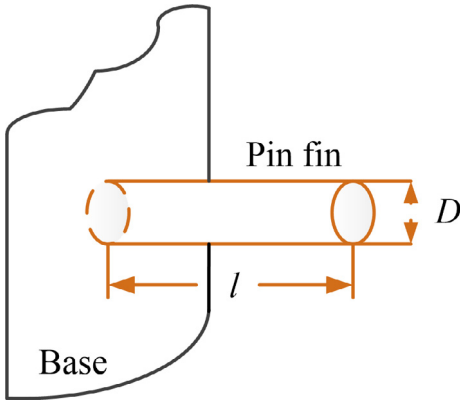

Fig. 11. Schematic of pin fin model.

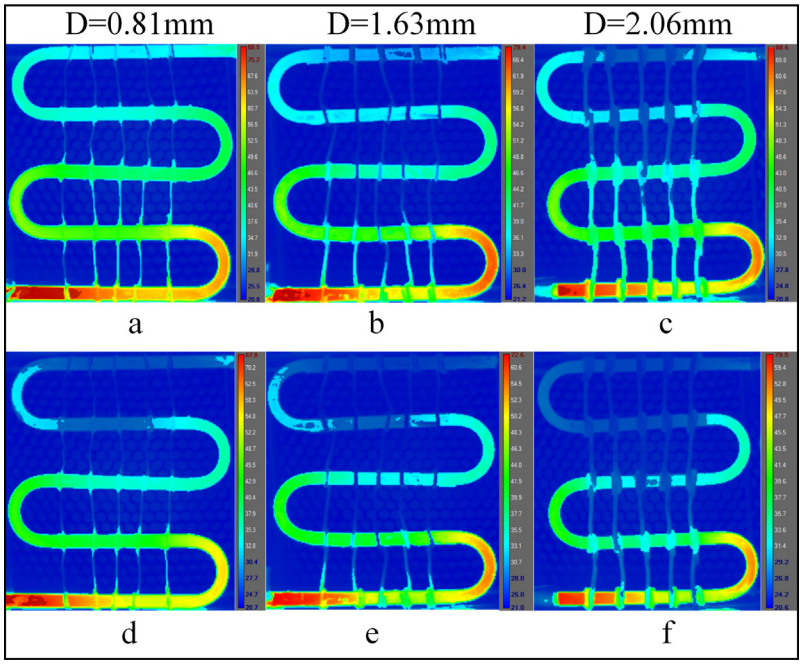

Fig. 10. Surface temperature distribution for tube-wire heat exchangers. (Tube inlet temperature: 150 °C, wind tunnel velocity: a–c: 8 m/s; d–f: 15 m/s).

tiled type for 14PPI and 20PPI heat exchangers have better heat transfer than that of 10PPI. The reason is that the 20PPI wire mesh has largest heat transfer surface area at the tube outside.

The tube outside Nusselt number variation with *Re* number for clamped SPW heat exchangers is plotted in Fig. 9. It can be seen that the heat transfer enhancement for three porosity SPW heat exchangers has nearly the same increase compared with the plain tube. The types of 14PPI and 20PPI can transfer much more heat than that of 10PPI. The maximum value of heat transfer enhancement is about 25.9% under the condition of 20 m/s wind tunnel velocity. Nearly half of the tube surface was connected with the wire mesh and the aluminum coating was filled at the gap between tube surface and wires. It is equivalent that the tube outside diameter increases and the heat transfer surface area enlarges. Thus, the outside tube heat transfer also improves compared with the plain tube as shown in the figure. The roughness of the tube backside surface extends after wrapped with wires. Then, the flow separation point steps back and most of the air accumulates at the back surface of the tube to form a wake in the downstream. Plain tube surface has less thermal resistance and most of heat is transferred through the leading edge surface. Furthermore, the increase of the thermal resistance between the tube and the coating can restrain the heat conduction. The heat transfer displays almost the identical trend for heat exchangers with different porosities of wire meshes.

Considering the Nusselt number comparison between the tiled and clamped type heat exchangers, the three clamped types generally show better heat transfer than that of tiled ones. Furthermore, the clamped 20PPI heat exchanger obtain the best heat transfer enhancement and the tiled 10PPI displays the worst. Two suggestions are adopted to explain the results: firstly, the dense aluminum coatings spayed on the tiled type tube increase the thermal surface between the tube and the air flowing through it. The connected wire mesh can generate large thermal contact resistance due to the less contact area; secondly, clamped type is good for the physically connection between the tube and wire mesh. The practical application should trade off two factors for fabricating better and compacter heat exchangers.

As the wire mesh consists of a certain number of aluminum wires, single wire can be wrapped to the tube to form tube-wire heat exchanger. One single wire temperature distribution can be significantly displayed through infrared camera and heat transfer enhancement is easy to be modeled for the future analysis. Fig. 10 shows the experimental surface temperature distribution for tube-wire heat exchangers under wind tunnel velocities of 8 m/s and 15 m/s. To eliminate the influence of different tube air inlet directions, the hot air inlet was set at the bottom of the wind tunnel, which is opposite to that of SPW heat exchangers. The heat transfer can be treated as the identical condition at two directions due to the uniform air flow in the wind tunnel. The figure displays that the real temperature has the same tendency with the calculated fin temperature variation. Thus, fin model can be applied to analyze the heat transfer enhancement for SPW heat exchangers.

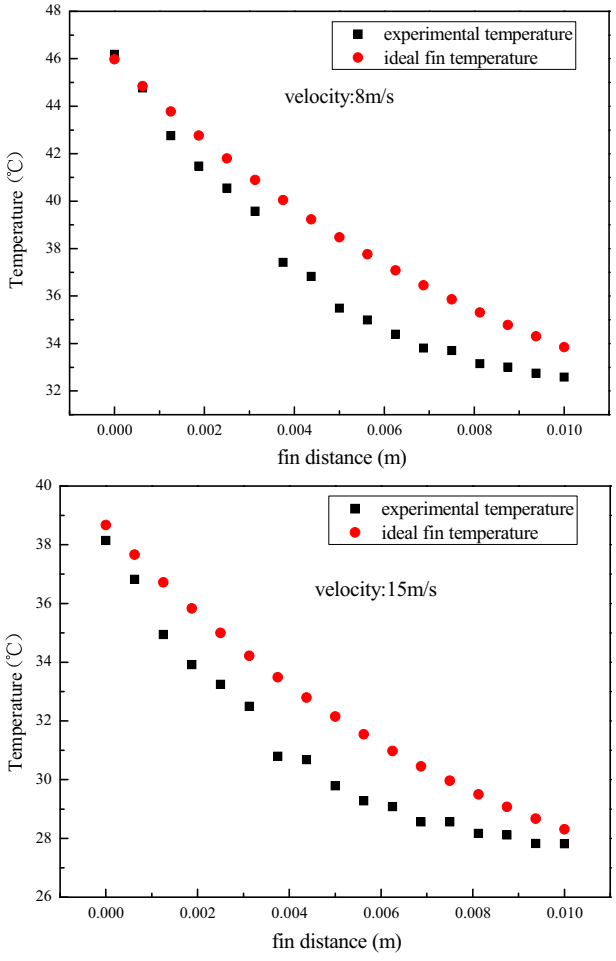

Fig. 12. Wire temperature variations for tube-wire heat exchanger and ideal fin model (wire diameter: 0.81 mm, wind tunnel velocity 8, 15 m/s).

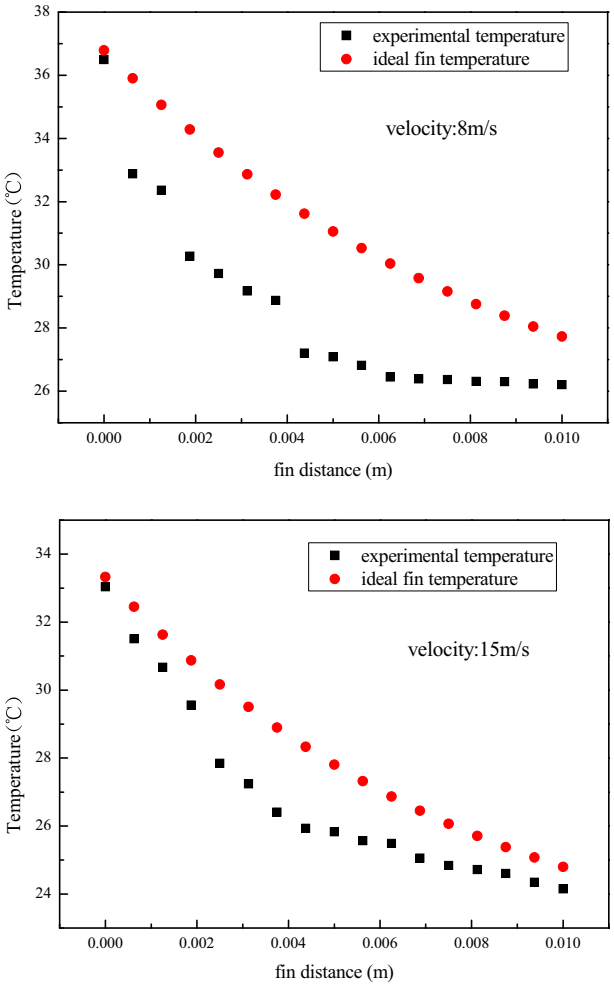

Fig. 13. Wire temperature variations for clamped 10PPI SPW heat exchanger and ideal fin model (wind tunnel velocity 8, 15 m/s).

3.3. Fin model explanation

The wire connection and sprayed coating can enlarge the heat transfer surface area compared with plain tube. As wire mesh was manufactured by warping aluminum wires, the wires can be considered as fins on the tube surface. The calculation of uniform cross section fins was used to compare with experimental results. The pin fins shown in Fig. 11 is applied and fin heat transfer rate q_f is the key factor to evaluate the enhancement of heat transfer. Convection heat transfer for the tip condition is used for simulation and fin heat transfer rate is defined as follows:

$$q_f = M\frac{\sinh ml + (h_m/m\lambda)\cosh ml}{\cosh ml + (h_m/m\lambda)\sinh ml} \tag{17}$$

The model fin length l is considered to be the tube bend radius. h_m is heat transfer coefficient flowing across the wire and can be solved using the empirical equation [35] as follows:

$$Nu_m = 0.683Re_m^{0.466}Pr_m^{1/3} \tag{18}$$

$$h_m = \frac{Nu_m\lambda_a}{D} \tag{19}$$

Reynolds number of wire mesh is calculated by wire diameter D and porosity ε as shown in Eq. (20).

$$Re_m = \frac{\rho uD}{\mu}\cdot(1-\varepsilon) \tag{20}$$

m and M are defined in following equations:

$$m = \sqrt{h_m P/\lambda A_c} \tag{21}$$

$$M = \sqrt{h_m P\lambda A_c}(\overline{T_s} - T_w) \tag{22}$$

P and A_c represent the wire perimeter and wire across section area, respectively. The base surface temperature T_s is obtained through infrared camera and average surface temperature $\overline{T_s}$ is calculated by integral averaging in terms of temperature distribution from tube inlet to outlet. To compare with fin surface temperature, wire temperature is analyzed through the camera pictures. The wire temperature using the fin model under the condition of convection is defined as the following equation:

$$\frac{T_x - T_\infty}{\overline{T_s} - T_\infty} = \frac{\cosh m(l-x) + (h_m/m\lambda)\sinh m(l-x)}{\cosh ml + (h_m/m\lambda)\sinh ml} \tag{23}$$

x represents the wire distance from the tube base and T_∞ is the wind tunnel air temperature.

3.4. Fin model comparison of SPW heat exchanger

Experimental wire and fin model calculated temperature distributions for tube-wire heat exchangers under two wind tunnel velocities are plotted in Fig. 12. The plots show that all the experimental wire temperatures are lower than those of ideal fin temperatures. The tube surface temperature can be considered as the base temperature of fin model. Experimental wire and fin model calculated temperature distributions for clamped 10PPI SPW heat exchanger under two wind tunnel velocities are displayed in Fig. 13. These distributions have the similar tendency with the tube-wire heat exchanger in Fig. 12. At the beginning of wire mesh, huge temperature drop happens due to the worse bonding than ideal model. Heat transfer to wires is limited because of the thermal contact resistance between the tube base and wires. As wire meshes are made up of many wires, more heat are transferred through the wire and fin model can be applied to the SPW heat exchangers. It is also concluded that the wire mesh heat transfer rate is less than the equivalent fins. Thus, heat transfer rate enhancement was defined as follows:

$$\Delta q = q_w - q_p \tag{24}$$

q_w and q_p represent the heat transfer rate for SPW heat exchanger and plain tube under same conditions, respectively. Thus, the efficiency of SPW heat exchanger is defined in the following equation:

$$\xi = \frac{\Delta q}{q_f} = \frac{q_w - q_p}{q_f} \tag{25}$$

Efficiencies of two types of SPW heat exchangers under various velocity conditions are plotted in Fig. 14. It is clearly seen that the bonding type and wire mesh porosity significantly affect the heat exchanger efficiency. The efficiency for each type heat exchangers is increasing under the velocity of 2 m/s–10 m/s and then becoming smoothly steady till to 20 m/s. The reason could be that experiments are performed with Reynolds number of wire mesh from 1000 to 11000 and the flow status is laminar. The efficiency is confined to the maximum of 76.7% under the 10 m/s condition with the increase of wind tunnel velocity. The figure also shows that clamped 20PPI SPW heat exchanger can achieve the highest heat transfer rate enhancement compared with others.

Furthermore, to predict the heat transfer of SPW heat exchangers, Nusselt number data is fitted with Reynolds number in terms of all experimental results. As wire mesh porosity and Reynolds number are the key factors to influence the Nusselt number, the fitting formula is presented as follows

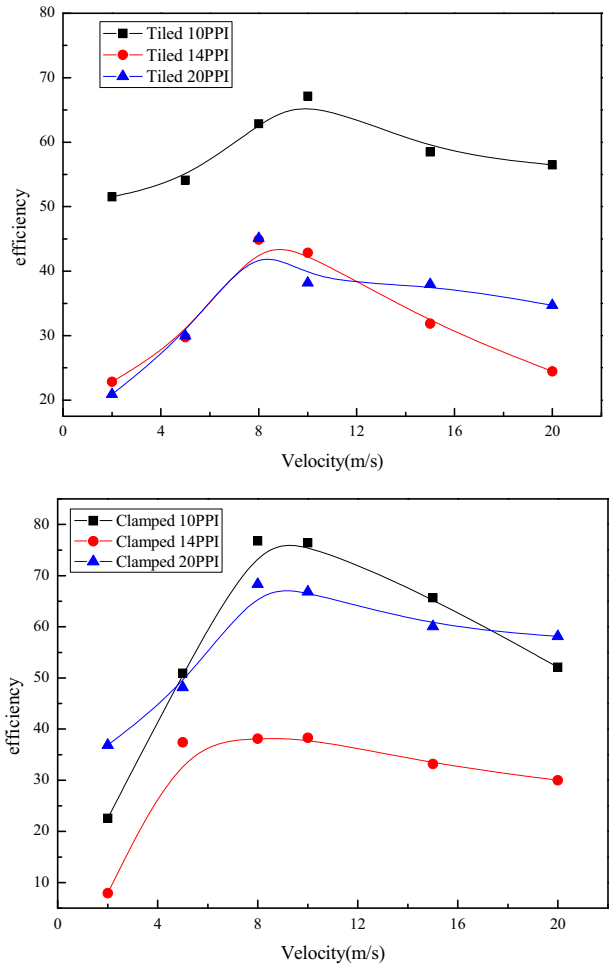

Fig. 14. SPW heat exchangers' efficiency under various wind tunnel velocities.

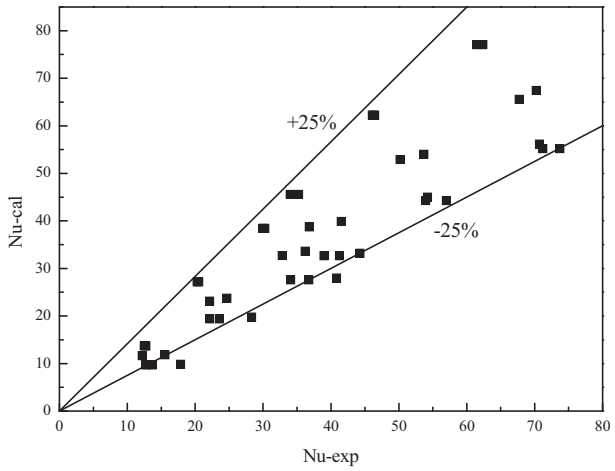

Fig. 15. Comparison between the calculated *Nu* number (Eq. (23)) and the experimental value.

$$Nu = 0.021 \cdot \frac{\varepsilon}{1-\varepsilon} Re_w^{0.75} Pr_w^{0.36} \tag{26}$$

Eq. (26) can be used to predict the tube outside heat transfer for tiled and clamped SPW heat exchangers. Fig. 15 shows the comparison between the calculated Nusselt numbers and all the experimental values. 96.2% of experimental points are within the ±25% error band and the average deviations is 19.2%.

4. Conclusions

Aluminum tube heat exchangers were fabricated by connecting aluminum wires and wire meshes with various porosities using wire-arc thermal spray system. Coating and connection quality, heat exchangers heat transfer rate and efficiencies were measured and analyzed in these series of experiments. The following conclusions have been made:

(1) Wire mesh could be connected well with tube by spraying Al coating in both clamped and tiled types.
(2) All SPW heat exchangers can enhance the heat transfer coefficient compared with plain tubes. The maximum value of heat transfer enhancement is about 25.9% for the clamped 20PPI SPW heat exchanger.
(3) Classic pin-fin model was verified using data of wire temperature distribution for tube-wire heat exchanger and the efficiency compared with ideal fin has the maximum value of 76.7% for all SPW heat exchangers under all experimental conditions.
(4) A correlation of tube outside Nusselt numbers of SPW heat exchangers were fitted with Reynolds number and it is used to predict the heat transfer enhancement.

References

[1] R. Shah, C.F. McDonald, C.P. Howard, Compact heat exchangers-history, technological advancement and mechanical design problems (1980).
[2] R. Shah, R. Webb, Compact and enhanced heat exchangers, Heat Exchangers: Theory and Practice, Begell House, USA, 1983, pp. 440–444.
[3] R.K. Shah, A.D. Kraus, D. Metzger, Compact Heat Exchangers (1990).
[4] Y. Yan, Z. Zhang, L. Zhang, X. Wang, K. Liu, Z. Yang, Investigation of autothermal reforming of methane for hydrogen production in a spiral multi-cylinder micro-reactor used for mobile fuel cell, Int. J. Hydrogen Energy 40 (4) (2015) 1886–1893.
[5] K. Boomsma, D. Poulikakos, F. Zwick, Metal foams as compact high performance heat exchangers, Mech. Mater. 35 (12) (2003) 1161–1176.
[6] L. Tadrist, M. Miscevic, O. Rahli, F. Topin, About the use of fibrous materials in compact heat exchangers, Exp. Therm. Fluid Sci. 28 (2) (2004) 193–199.
[7] J.-P. Bonnet, F. Topin, L. Tadrist, Flow laws in metal foams: compressibility and pore size effects, Transport Porous Med. 73 (2) (2008) 233–254.
[8] R. Kurian, C. Balaji, S. Venkateshan, Experimental investigation of near compact wire mesh heat exchangers, App. Therm. Eng. 108 (2016) 1158–1167.
[9] S. Mancin, C. Zilio, A. Diani, L. Rossetto, Experimental air heat transfer and pressure drop through copper foams, Exp. Therm. Fluid Sci. 36 (2012) 224–232.
[10] M. White, G. Nellis, S. Klein, W. Zhu, Y. Gianchandani, An experimentally validated numerical modeling technique for perforated plate heat exchangers, J. Heat Trans.-T ASME 132 (11) (2010) 111801.
[11] W. Wu, J. Liu, W. Li, W. Hsieh, Measurement and correlation of hydraulic resistance of flow through woven metal screens, Int. J. Heat Mass Transfer 48 (14) (2005) 3008–3017.
[12] V. Calmidi, R. Mahajan, Forced convection in high porosity metal foams, J. Heat Trans.-T ASME 122 (3) (2000) 557–565.
[13] J.J. Hwang, G.J. Hwang, R.H. Yeh, C.H. Chao, Measurement of interstitial convective heat transfer and frictional drag for flow across metal foams, J. Heat Trans.-T ASME 124 (1) (2002) 120.
[14] W.H. Hsieh, J.Y. Wu, W.H. Shih, W.C. Chiu, Experimental investigation of heat-transfer characteristics of aluminum-foam heat sinks, Int. J. Heat Mass Transfer 47 (23) (2004) 5149–5157.
[15] N. Dukhan, K.-C. Chen, Heat transfer measurements in metal foam subjected to constant heat flux, Exp. Therm. Fluid Sci. 32 (2) (2007) 624–631.
[16] J. Sodre, J. Parise, Friction factor determination for flow through finite wire-mesh woven-screen matrices, J. Fluids Eng. 119 (4) (1997) 847–851.
[17] L. Varshney, J. Saini, Heat transfer and friction factor correlations for rectangular solar air heater duct packed with wire mesh screen matrices, Sol. Energy 62 (4) (1998) 255–262.
[18] R. Karabacak, G. Yakar, Forced convection heat transfer and pressure drop for a horizontal cylinder with vertically attached imperforate and perforated circular fins, Energy Convers. Manage. 52 (8–9) (2011) 2785–2793.
[19] D.H. Lee, J.M. Jung, J.H. Ha, Y.I. Cho, Improvement of heat transfer with perforated circular holes in finned tubes of air-cooled heat exchanger, Int. Commun. Heat Mass. 39 (2) (2012) 161–166.
[20] Y. Liu, G. Xu, X. Luo, H. Li, J. Ma, An experimental investigation on fluid flow and heat transfer characteristics of sintered woven wire mesh structures, Appl. Therm. Eng. 80 (2015) 118–126.
[21] G.-m. Zhang, G.-q. Li, W. Li, Z. Zhang, X.-l. Leng, M.-c. Tian, Particulate fouling and composite fouling assessment in corrugated plate heat exchangers, Int. J. Heat Mass Transfer 60 (2013) 263–273.
[22] J. Xu, J. Tian, T.J. Lu, H.P. Hodson, On the thermal performance of wire-screen meshes as heat exchanger material, Int. J. Heat Mass Transfer 50 (5–6) (2007) 1141–1154.
[23] S. Mancin, C. Zilio, A. Diani, L. Rossetto, Air forced convection through metal foams: Experimental results and modeling, Int. J. Heat Mass Transfer 62 (2013) 112–123.
[24] S.C. Costa, H. Barrutia, J.A. Esnaola, M. Tutar, Numerical study of the pressure drop phenomena in wound woven wire matrix of a Stirling regenerator, Energy Convers. Manage. 67 (2013) 57–65.
[25] J. White, CFD Simulation and Experimental Comparison of a Copper Wire Woven Finned Heat Exchanger to an Aluminium Flat Plate Finned Heat Exchanger (2013).
[26] S.S. Feng, J.J. Kuang, T. Wen, T.J. Lu, K. Ichimiya, An experimental and numerical study of finned metal foam heat sinks under impinging air jet cooling, Int. J. Heat Mass Transfer 77 (2014) 1063–1074.
[27] W. Li, H.-x. Li, G.-q. Li, S.-c. Yao, Numerical and experimental analysis of composite fouling in corrugated plate heat exchangers, Int. J. Heat Mass Transfer 63 (2013) 351–360.
[28] K. Boomsma, D. Poulikakos, On the effective thermal conductivity of a three-dimensionally structured fluid-saturated metal foam, Int. J. Heat Mass Transfer 44 (4) (2001) 827–836.
[29] S. Mahjoob, K. Vafai, A synthesis of fluid and thermal transport models for metal foam heat exchangers, Int. J. Heat Mass Transfer 51 (15–16) (2008) 3701–3711.
[30] H.S. Jazi, J. Mostaghimi, S. Chandra, L. Pershin, T. Coyle, Spray-formed, metal-foam heat exchangers for high temperature applications, J. Therm. Sci. Eng. Appl. 1 (3) (2009) 031008.
[31] N. Tsolas, S. Chandra, Forced convection heat transfer in spray formed copper and nickel foam heat exchanger tubes, J. Heat Trans.-T ASME 134 (6) (2012) 062602.
[32] R. Rezaey, S. Salavati, L. Pershin, T. Coyle, S. Chandra, J. Mostaghimi, Fabrication of wire mesh heat exchangers for waste heat recovery using wire-arc spraying, J. Therm. Spray Technol. 23 (4) (2014) 609–615.
[33] V. Gnielinski, New equations for heat and mass-transfer in turbulent pipe and channel flow, Int. Chem. Eng. 16 (2) (1976) 359–368.
[34] A. Zukausras, Heat transfer from tubes in crossflow, Adv. Heat Transfer 8 (1973) 93.
[35] Y.A. Cengel, S. Klein, W. Beckman, Heat Transfer: A Practical Approach, WBC McGraw-Hill Boston, 1998.